Geometric and electronic structures of hydrogenated transition metal (Sc, Ti, Zr) clusters

T. J. Dhilip Kumar, P. Tarakeshwar,* and N. Balakrishnan†
Department of Chemistry, University of Nevada Las Vegas, 4505 Maryland Parkway, Las Vegas, Nevada 89154, USA
(Received 3 December 2008; published 18 May 2009)

We report first-principles electronic structure calculations of hydrogen adsorption and saturation on M_{13} (M=Sc,Ti,Zr) clusters of icosahedral (I_h) and cuboctahedral (O_h) symmetries. Hydrogen saturation of the I_h metal clusters yields energetically stable $M_{13}H_{20}$ and $M_{13}H_{30}$ systems compared to $M_{13}H_{14}$ and $M_{13}H_{24}$ systems for O_h clusters. In all these clusters, the hydrogen adsorption involves dissociative chemisorption of H_2 molecules. Upon initial hydrogenation, the dissociated hydrogen atoms lie above either the triangular or quadrangular face of the metal cluster. A further increase in hydrogen saturation leads to the formation of bridged hydrogen bond between adjacent metal atoms. The role of the unfilled *d* orbitals in imparting stability to the hydrogenated clusters is explored by examining their density of states (DOS) near the Fermi level. It has been found that the inverse correlation between the *d*-band center and the chemisorption energies is valid only at low hydrogen concentrations. At higher hydrogen coverages, the trend is reversed. The results illustrate that at high adsorbate concentrations or surface coverage, the correlation of the chemisorption energies with the *d*-band center of the pure metal cluster or nanoparticle may not be realistic but one has to take into account the changes in the *d*-orbital DOS due to the presence of coadsorbed molecules. To obtain further insights into the initial steps involved in hydrogen adsorption and dissociation, the transition states and activation energies of the $M_{13}H_2$ system have been determined and found to conform with the empirical Brønsted-Evans-Polanyi relationship. A highly intense infrared band in the 1000–1500 cm^{-1} region, associated with the adsorbed hydrogens in these hydrogenated metal clusters, may be used to experimentally monitor hydrogen coverage.

DOI: 10.1103/PhysRevB.79.205415 PACS number(s): 36.40.−c, 71.15.Ap, 82.33.Hk, 61.46.Bc

I. INTRODUCTION

Transition metal clusters have attracted much attention recently because of their utility as nanocatalysts and scaffolds for functional nanomaterials.[1–4] Owing to their efficacy in the design and development of novel nanomaterials for hydrogen storage, there has been an increased interest in understanding the interaction of hydrogen with metal clusters.[5] Hydrogen storage on metal clusters is also of interest because recent experimental studies suggest that for some metal systems, nanoparticles exhibit a higher affinity for hydrogen than the corresponding bulk materials.[6]

A number of recent studies have investigated the usefulness of titanium-decorated organic molecules or nanostructured materials such as graphene, carbon nanotubes, and fullerenes as potential materials for hydrogen storage.[7–12] It has been argued that the tendency of titanium atoms to form energetically stable clusters may limit their applicability as dopants in hydrogen storage materials.[13] This brings the important issue of metal clustering and cluster stability in transition metal–decorated hydrogen storage materials.[14,15] Exposure to high concentrations of H_2 may also induce structural changes in the parent cluster. Thus, a detailed investigation of energetics of hydrogen adsorption and desorption on metal clusters as well as any structural changes during hydrogenation/dehydrogenation cycles would be valuable in designing viable metal-doped hydrogen storage materials. It should be noted that any practical hydrogen storage material must (i) display favorable enthalpies for hydrogen absorption and desorption, (ii) enable quick uptake and release, (iii) exhibit high storage capacity, (iv) provide effective heat transfer, (v) have small volumes and be lightweight, (vi) form stable complexes with hydrogen, (vii) be durable and exhibit high mechanical strength, and (viii) be safe.[16] Recent studies of hydrogen adsorption on metal nanoparticles focused on clusters containing heavy metals such as gold, palladium, and platinum.[17–20] The few studies on light metal clusters were restricted to theoretical investigations of aluminum clusters.[21–23] Here we examine hydrogen adsorption, saturation, and bonding characteristics of some of the early transition metal clusters in isolation.

Our interest in hydrogen adsorption on isolated metal clusters is also motivated in part by recent experimental observations which indicate that scandium, titanium, and zirconium metals are excellent catalysts for the hydrogenation and dehydrogenation kinetics of complex metal hydrides such as $NaAlH_4$.[24–32] In particular, it has been found that nanoparticles of these metals are better catalysts than the corresponding bulk metal.[30] However, most theoretical studies appear to limit the role of the metal catalysts to dissociating molecular hydrogen in complex metal hydrides.[33–45] Recent studies have indicated that small icosahedral titanium clusters form stable hydrogen-saturated complexes.[46–48] In this paper we investigate icosahedral and cuboctahedral clusters of Sc, Ti, and Zr and examine if this is a general phenomenon exhibited by neighboring elements of titanium from the same row or group. In the absence of any experimental and theoretical studies of hydrogen adsorption and saturation on these metal clusters, we compare and contrast our findings with the more widely studied aluminum clusters.[21,22]

Electronic structures of isolated and hydrogen-loaded titanium clusters have been the topic of a number of recent investigations.[46–51] To the best of our knowledge, effects of hydrogen adsorption and saturation have not been investigated for zirconium or scandium clusters. However, electronic structures of isolated zirconium and scandium clusters have been the focus of some recent theoretical studies.[52–54]

Our work on bare titanium clusters showed that the 13-atom distorted icosahedral cluster[46] is exceptionally stable, in agreement with experimental observations.[55,56] Interestingly, studies on bare scandium and zirconium clusters also indicate high energetic stability for the 13-atom icosahedral clusters. The work on Sc_{13} reveals that the binding energies for spin multiplicities ranging from 2 to 20 are nearly similar.[53]

It is pertinent to note that cuboctahedral or icosahedral shapes are preferentially formed in cluster growth leading to magic number clusters (7, 13, 55, etc.), and they generally correspond to the global minima in structural optimizations.[57,58] Moreover at high temperatures, bulk metals energetically prefer icosahedral or bcc symmetries which are an extended form of cuboctahedral symmetry.[59] This observation is relevant to the present work because most experimental studies of hydrogenation and dehydrogenation involve high temperatures and pressures.

For the reasons mentioned above and for computational ease, the present study is restricted to 13-atom icosahedral or cuboctahedral metal clusters. We employ density functional theory (DFT) methods to evaluate the optimum structures and energetics of hydrogenated clusters. We calculate the activation energies for initial hydrogen adsorption on Ti, Sc, and Zr clusters by mapping the reaction path and analyzing the corresponding transition states. In Sec. II, we provide an overview of the computational methods employed and discuss the results for the bare and hydrogenated M_{13} clusters. A summary of our findings is given in Sec. IV.

II. COMPUTATIONAL DETAILS

The electronic structure calculations were carried out using DFT with the generalized gradient approximation (GGA) of Perdew and Wang (PW91).[60] The single-particle Kohn-Sham equations were solved using the plane-wave-based Vienna *ab initio* simulation program (VASP).[61–64] The interactions between the ions and valence electrons were described by the projector-augmented wave (PAW) method[65] as described by Kresse and Joubert.[66] For the plane-wave basis set a cutoff energy of 400 eV was used. Only the gamma point was needed for the finite systems considered here. All clusters were simulated by placing them at the center of cubic supercells that are large enough to neglect cluster-cluster interactions. The size of the unit cell was chosen such that the distance between neighboring images was more than 20 Å. This choice was shown to be sufficient to eliminate the interaction between neighboring images. Full geometry relaxation was performed for both the bare and hydrogenated metal clusters. Optimization of static structures were accomplished by moving atoms to the positions at which all atomic forces were <0.02 eV/Å. Parameters such as the cutoff energy and the size of unit cell were tested and optimized for securing converged results. The efficacy of VASP-based DFT methods in obtaining reliable electronic structures and properties of hydrogen storage materials has recently been documented.[67]

The binding energy per atom of M_{13} clusters, where M = Al, Sc, Ti, and Zr, is obtained by

$$\Delta E_{\mathrm{BE}} = (1/13)[13E_M - E_{M_{13}}]. \quad (1)$$

The average dissociative chemisorption energy of $M_{13}H_n$ clusters is calculated by

$$\Delta E_{\mathrm{CE}} = (2/n)[E_{M_{13}} + (n/2)E_{\mathrm{H}_2} - E_{M_{13}\mathrm{H}_n}], \quad (2)$$

where $n=2$, 20, and 30 for I_h clusters and 14, and 24 for O_h clusters considered in this study. $E_{M_{13}}$ is the electronic energy of the isolated clusters, E_{H_2} is the energy of H_2 molecule, and $E_{M_{13}\mathrm{H}_n}$ is the total energy of the cluster with n adsorbed hydrogen atoms.

The sequential desorption energy per hydrogen atom is defined as

$$\Delta E_{\mathrm{DE}} = E_{\mathrm{H}} + (1/2)[E_{M_{13}\mathrm{H}_{n-2}} - E_{M_{13}\mathrm{H}_n}], \quad (3)$$

where $n=2,4,6,\ldots,30$.

To provide mechanistic insights into the hydrogenation process, we computed the transition states and the corresponding activation energies using the linear synchronous transit (LST) method[68] implemented in the DMOL program.[69] In the LST method, the minimum-energy path between reactants and products is interpolated by performing a LST maximization. The LST calculations were performed using DFT within the GGA with the PW91 functional. Double numerical basis sets augmented with polarization functions (DNPs) were utilized to describe all the electrons of scandium and titanium and the valence electrons in zirconium. Effective core potentials were used to describe the core electrons in zirconium. For the sake of comparison, calculations including effective core potentials were also carried out for the titanium clusters.

III. RESULTS AND DISCUSSION

A. Isolated M_{13} clusters

As discussed in Sec. II, 13-atom magic number clusters have an energetic preference for globular geometries possessing icosahedral or cuboctahedral symmetries. Our calculations of the isolated metal clusters indicate small distortions from the perfect icosahedral (I_h) symmetry. However, there are no distortions for the cuboctahedral (O_h) symmetry. Similar distortions from the perfect icosahedron have been noted in earlier studies of the isolated Ti_{13} cluster.[70,71] The main difference between the icosahedral and the octahedral symmetries is that the former is comprised of 20 triangular faces, 30 edges, and 12 vertices, while the latter has 6 quadrangular faces, 8 triangular faces, 24 edges, and 12 vertices. This difference has a bearing on the hydrogen adsorption and saturation abilities of these clusters.

The binding energies per atom of Sc, Ti, and Zr clusters of I_h and O_h symmetries are tabulated in Table I. The binding energies of Ti_{13} and Zr_{13} clusters are much higher than that of Sc_{13} and Al_{13} clusters. This can be attributed to the increased availability of d electrons for bonding in Ti and Zr clusters.[72] The presence of more nearest neighbors around each atom in the I_h clusters and the energetic stabilization accruing from an increased hybridization of the available p or d electrons account for their enhanced stability over the corresponding O_h clusters. Similar energetic trends for I_h geometries have been found in other metal clusters such as

TABLE I. Energetics of M_{13} clusters of Al, Sc, Ti, and Zr with I_h and O_h symmetries.

	Icosahedral symmetry		Cuboctahedral symmetry	
System	ΔE_{BE} (eV)	ΔE_g [a] (eV)	ΔE_{BE} (eV)	ΔE_g [a] (eV)
Al_{13}	2.57	1.96 (1.93)	2.50	1.25 (1.13)
Sc_{13}	2.94	0.62 (0.41)	2.76	0.31 (0.23)
Ti_{13}	4.35	1.11 (0.96)	4.14	0.63 (0.36)
Zr_{13}	4.63	1.27 (0.25)	4.32	0.20 (0.20)

[a]The highest occupied molecular orbital (HOMO)–lowest unoccupied molecular orbital (LUMO) gaps are the difference between the energies of the highest singly occupied molecular orbital (SOMO) and the lowest-energy unoccupied orbital of the same spin (spin-up configuration). The values in parentheses correspond to the evaluated HOMO-LUMO gap, irrespective of the spin.

Fe_{13},[73] Ru_{13}, Rh_{13}, and Pd_{13}.[74] When the number of d electrons increases, the increased hybridization leads to the occupation of the destabilizing antibonding orbitals and consequently O_h geometries are more stable for Pt_{13} (Ref. 75) and Au_{13} (Ref. 76) clusters.

The calculated HOMO-LUMO gaps ΔE_g are shown in Table I. The magnitudes of the gaps for some of the clusters such as the I_h Al_{13} are in agreement with recent studies.[22,77,78] It should be noted that a few earlier studies have reported much smaller gaps for this system,[79,80] the reasons for which have been elaborated in a recent and detailed study of I_h Al_{13}.[78]

B. $M_{13}H_n$ clusters

Earlier studies by Goldberg and Yarovsky[22] indicated that $Al_{13}H_m$ (m=20,30,42) clusters are energetically not stable because of the presence of imaginary frequencies in the ground-state configuration. Therefore, they carried out calculations on the corresponding $Al_{12}H_{12}$ and $Al_{12}H_{20}$ clusters,[22] wherein the central metal atom was removed. However for titanium-containing clusters, our recent studies have shown that hydrogen molecules undergo dissociative chemisorption as they approach the metal cluster at close proximity.[48] The high stability of these hydrogen saturated clusters was further confirmed by the absence of imaginary frequencies in the Hessian, indicating that they correspond to minimum-energy configurations. The dissociated hydrogen atoms lie either above the center of the triangular face of three titanium atoms or above the bond connecting two titanium atoms, depending on the degree of hydrogen saturation. Unlike hydrogenated aluminum clusters,[22] structures possessing terminal Ti-H bonds were found to be energetically unstable.[47] Recent studies have indicated that hydrogen dissociation on platinum clusters also lead to similar two-center (μ_2) or three-center (μ_3) bonding motifs.[81,82] A two-center site corresponds to the hydrogen lying above the bridge between two metal atoms, and a three-center site corresponds to the hydrogen forming an apex to three metal atoms.

Like small titanium clusters, hydrogen adsorption on both I_h and O_h M_{13} (M=Sc,Zr) clusters involves dissociative chemisorption. For I_h clusters, the dissociated hydrogen atom initially binds to the triangular face formed by three apex metal atoms. For O_h clusters, the hydrogen atom binds to the triangular or quadrangular face formed by three or four metal atoms. This leads to the formation of $M_{13}H_{20}$ and $M_{13}H_{14}$ clusters [Figs. 1(a) and 1(b)]. Our recent investigation of sequential dissociative chemisorption of H_2 on I_h Ti_{13} clusters showed that at low hydrogen concentrations, structures possessing singly bonded Ti-H or twofold hydrogen-bonding motifs were energetically less stable than those with threefold bonding motifs,[47] similar to that observed for hydrogen adsorption on platinum clusters.[82] Interestingly, μ_4-type hydrogen bonding has also been observed in octahedral Pt_{13},[75] boron,[83] and yttrium clusters.[84] As the hydrogen concentration is increased, a transition from μ_3 or μ_4 to μ_2 bonding occurs, leading to $M_{13}H_{30}$ (I_h) and $M_{13}H_{24}$ (O_h) clusters [Figs. 1(c) and 1(d)]. The energetic changes accompanying μ_3 (H_{20}) to μ_2 (H_{30}) transition has been elaborated in our recent study of hydrogen saturation of I_h Ti_{13} cluster.[47]

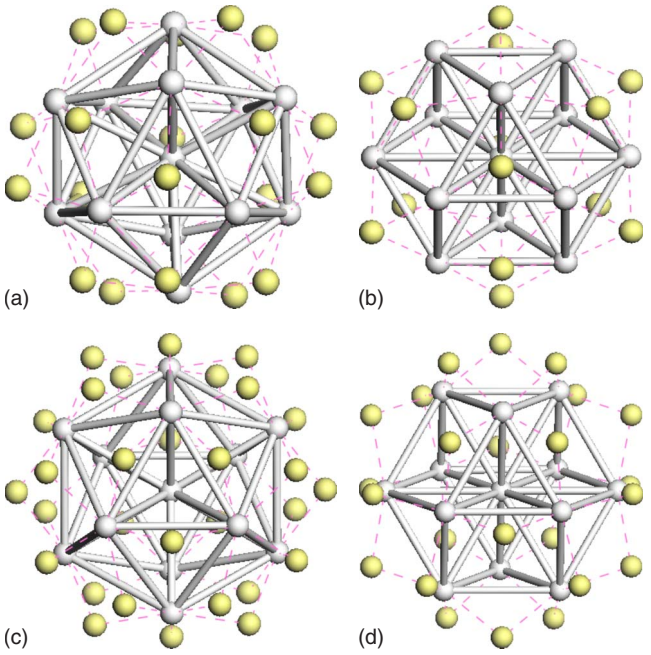

FIG. 1. (Color online) Optimized structures of hydrogenated (a) I_h $Zr_{13}H_{20}$, (b) O_h $Zr_{13}H_{14}$, (c) I_h $Zr_{13}H_{30}$, and (d) O_h $Zr_{13}H_{24}$ clusters. The other hydrogenated metal clusters have similar structures.

In Table II, we provide the average bond lengths between central (M_c) and apex (M_a) metal atoms in isolated M_{13} and hydrogenated M_{13} clusters of I_h and O_h geometries. It can be noted that at low or moderate hydrogen concentrations ($M_{13}H_{20}$), the geometry of the metal cluster is unaffected by hydrogen loading. However at higher hydrogen concentrations ($M_{13}H_{30}$), there is a slight elongation of the M_c-M_a bonds. The trends in the bond lengths indicate similarities between aluminum and titanium and scandium and zirconium. The similarity of the electronic spatial extent of the d orbitals of scandium and zirconium can be expected from their similar atomic radii, which is 1.62 Å for Sc and 1.60 Å for Zr. Similarly, titanium and aluminum with their comparable atomic radii of 1.47 and 1.43 Å would lead to

TABLE II. Comparison of the bond lengths of the isolated and hydrogenated I_h and O_h $M_{13}H_n$ clusters of Al, Sc, Ti, and Zr.

System	M_a-M_c (pm)	M_a-M_a (pm)
	Icosahedral clusters	
Al_{13}	267	281
Sc_{13}	291	313
Ti_{13}	262	276
Zr_{13}	286	301
$Sc_{13}H_{20}$	290	304
$Ti_{13}H_{20}$	264	275
$Zr_{13}H_{20}$	292	310
$Sc_{13}H_{30}$	326	342
$Ti_{13}H_{30}$	279	293
$Zr_{13}H_{30}$	309	325
	Cuboctahedral clusters	
Al_{13}	273	273
Sc_{13}	296	296
Ti_{13}	264	264
Zr_{13}	296	296
$Sc_{13}H_{14}$	300	300
$Ti_{13}H_{14}$	264	264
$Zr_{13}H_{14}$	295	295
$Sc_{13}H_{24}$	320	320
$Ti_{13}H_{24}$	275	275
$Zr_{13}H_{24}$	306	306

TABLE III. Energetics of $M_{13}H_n$ clusters of Al, Sc, Ti, and Zr with I_h and O_h symmetries.

System	ΔE_{CE} (eV)	ΔE_g [a] (eV)
	Icosahedral clusters	
$Al_{13}H_{20}$	0.33	0.87 (0.36)
$Sc_{13}H_{20}$	2.20	0.83 (0.66)
$Ti_{13}H_{20}$	1.99	1.01 (0.60)
$Zr_{13}H_{20}$	1.81	0.92 (0.47)
$Al_{13}H_{30}$		
$Sc_{13}H_{30}$	0.96	1.21 (0.66)
$Ti_{13}H_{30}$	1.15	1.11 (0.37)
$Zr_{13}H_{30}$	1.35	1.41 (0.33)
	Cuboctahedral clusters	
$Al_{13}H_{14}$	0.22	0.76 (0.17)
$Sc_{13}H_{14}$	1.89	0.78 (0.34)
$Ti_{13}H_{14}$	1.99	0.86 (0.72)
$Zr_{13}H_{14}$	1.86	0.86 (0.68)
$Al_{13}H_{24}$	0.16	0.88 (0.11)
$Sc_{13}H_{24}$	1.57	0.62 (0.26)
$Ti_{13}H_{24}$	1.79	1.29 (1.29)
$Zr_{13}H_{24}$	1.94	1.53 (1.53)

[a]The HOMO-LUMO gaps are the difference between the energies of the SOMO and the lowest-energy unoccupied orbital of the same spin (spin-up configuration). The values in parentheses correspond to the evaluated HOMO-LUMO gap, irrespective of the spin.

smaller electronic spatial extents of their d and p orbitals. The spatial extents of the orbital and the bond lengths are correlated because the stabilization of the hydrogen atom in these metal clusters results from the in-phase interaction of the atomic orbitals comprised of the 1s orbital of the hydrogen atom and the hybridized s and d orbitals of the metal atoms. This is somewhat akin to the stabilization of hydrogen atoms bound through three-center four-electron (3c-4e) bonds in boranes,[85] wherein the hydrogen atom is located at the intersection of the three boron p orbitals.

At low hydrogen concentrations, the average chemisorption energies per H_2 molecule for both the hydrogenated O_h and I_h clusters are similar (Table III). However at higher hydrogen loading, the O_h clusters display much higher chemisorption energies than the corresponding I_h clusters, though the latter adsorb three more hydrogen molecules than the former. Although the binding energies of the isolated O_h clusters are lower than that of the corresponding I_h clusters, the results indicate that the energetic stability of the parent cluster has little bearing on the chemisorption energies at high hydrogen concentrations. While we could not optimize an I_h $Al_{13}H_{30}$ cluster, it can be noted that the chemisorption energies of the hydrogenated aluminum clusters are much lower than all of the other clusters investigated in this study. An increase in hydrogen concentration beyond 30 hydrogen atoms leads to a dramatic decrease in the hydrogen chemisorption energies, with many of the hydrogen molecules being adsorbed in undissociated form.[47] Hence, we believe that these hydrogen concentrations are the optimal limits for the formation of energetically stable hydrogenated metal clusters.

Earlier theoretical work on zirconium clusters indicated that spin-orbit effects are small.[86–88] But it is known that relativistic and spin-orbit effects become important in calculations involving second-row and heavier transition metals. Therefore we carried out calculations on the icosahedral $Zr_{13}H_{20}$ cluster by explicitly taking into account spin-orbit coupling using the method described by Hobbs *et al.*[89] This yielded an average chemisorption energy of 1.81 eV, in agreement with that obtained in calculations without including spin-orbit effects (Table III). Thus, the effect of spin-orbit coupling is negligible, in accordance with earlier theoretical work on zirconium clusters.[86–88] Based on these results, spin-orbit coupling was not included in all other calculations reported here. We have also verified that the minimum-energy geometries of $Zr_{13}H_{20}$ optimized with and without spin-orbit coupling are similar.

Since the hydrogenated metal clusters are characterized by different types of bonding motifs (μ_2, μ_3, μ_4) depending on the degree of hydrogen saturation and the geometry of the cluster, it would be useful to examine the variation in the chemisorption energy with respect to the bonding pattern and the nature of the metal atom. This is shown in Table IV for

TABLE IV. Calculated chemisorption energies of μ_2, μ_3, and μ_4 metal-hydrogen-bonded O_h M_{13} (M=Sc,Ti,Zr) clusters.

System	ΔE_{CE} (eV)
μ_2	
$Sc_{13}H_{24}$	1.57
$Ti_{13}H_{24}$	1.79
$Zr_{13}H_{24}$	1.94
μ_3	
$Sc_{13}H_8$	2.06
$Ti_{13}H_8$	2.09
$Zr_{13}H_8$	2.03
μ_4	
$Sc_{13}H_6$	1.85
$Ti_{13}H_6$	1.66
$Zr_{13}H_6$	1.67

O_h clusters of the three metals. The results show that for $M_{13}H_8$ clusters which are characterized by μ_3 hydrogens, the chemisorption energy is insensitive to the nature of the metal atom. Interestingly, both titanium and zirconium clusters exhibit similar chemisorption energies for hydrogens binding to the μ_4 site ($M_{13}H_6$). The higher chemisorption energies of the hydrogenated scandium clusters for this bonding motif can be attributed to the greater contribution of the spherically symmetric s orbital of the hybridized s-d orbitals. On a similar note, the enhanced contribution of the directional d orbital to the hybridized s-d orbitals leads to the larger chemisorption energies of the titanium and zirconium clusters characterized by μ_2 hydrogens ($M_{13}H_{24}$). The difference between the μ_3 and μ_4 bonding motifs can also be inferred from the slices of the electron density of the $Ti_{13}H_8$ and $Ti_{13}H_6$ clusters shown in Fig. 2. The polarization of the spherically symmetric H s orbital is seen to be more pronounced for $Ti_{13}H_8$ than $Ti_{13}H_6$. The enhanced energetic stabilization accruing from this polarization is manifested in the larger chemisorption energies of the $Ti_{13}H_8$ cluster.

Against this background, it is useful to examine the modulation of the chemisorption [Eq. (2)] and sequential desorption [Eq. (3)] energies as functions of the number of hydrogen atoms. The results are shown in Fig. 3 along with similar results obtained using the DMOL program.[47] It can be noted from Fig. 3 that both the current VASP and earlier DMOL calculations yield similar results and that the chemisorption energies decrease as the number of H_2 molecules interacting with the Ti_{13} cluster is steadily increased. The sequential desorption energy per H atom is higher than the chemisorption energy because the former is defined with respect to the energy of the dissociated H atom, while the latter is calculated with respect to the energy of the intact hydrogen molecule. While the trends in desorption energy mirror that of the chemisorption energy, the former curve exhibits several spikes in the transition from $Ti_{13}H_{20}$ to $Ti_{13}H_{30}$. This results from the enhanced energetic stability/instability of some of the intervening clusters. It can also be noted that more energy has to be expended to desorb hydrogens from the $Ti_{13}H_{20}$ than from the $Ti_{13}H_{30}$ cluster. This is due to the enhanced energetic stability of μ_3 hydrogens as compared to the μ_2 hydrogens.

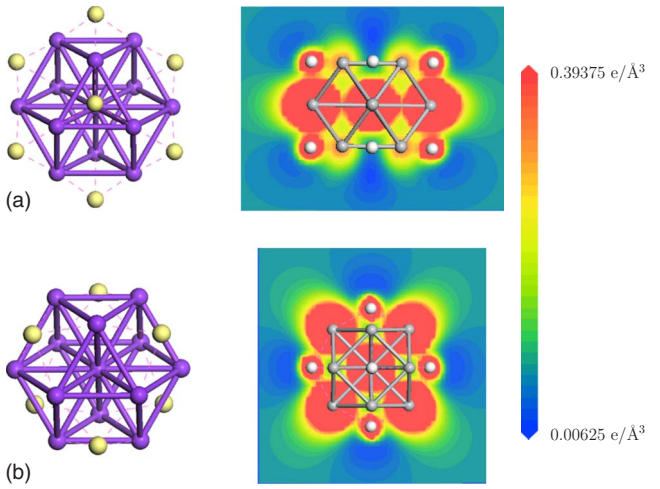

FIG. 2. (Color online) Optimized structures and electronic charge densities of (a) $Ti_{13}H_8$ (μ_3) and (b) $Ti_{13}H_6$ (μ_4) clusters. The charge densities shown in (a) are plotted in a plane bisecting the $Ti_{13}H_8$ cluster and containing three titanium and four hydrogen atoms. The charge densities shown in (b) are plotted in a plane bisecting the $Ti_{13}H_6$ cluster and containing five titanium and four hydrogen atoms.

C. Chemisorption energy versus d-band center

To provide further insight into the nature of bonding in the hydrogenated clusters, the total densities of states (DOSs) and partial DOSs of the central metal atom in both the I_h and O_h clusters are shown in Figs. 4 and 5. For comparison we also included results for $Al_{13}H_{24}$. For the aluminum cluster, the contribution of the occupied orbitals to the total DOS near the Fermi level (E_F) is small. Furthermore, the central Al atom has virtually no contribution to the DOS at the Fermi level and therefore plays no role in stabilizing the cluster. This also explains the relative stability of the corresponding Al_{12} clusters.[22]

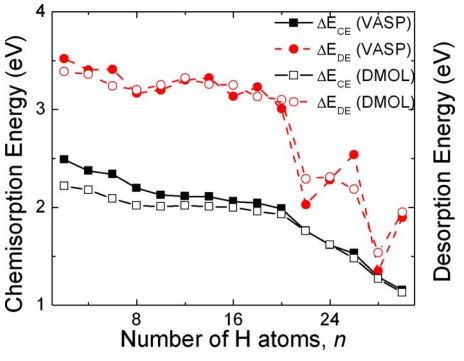

FIG. 3. (Color online) Calculated VASP and DMOL (10 Å basis cutoff) chemisorption (ΔE_{CE}) and sequential desorption (ΔE_{DE}) energies of $Ti_{13}H_n$ (n=2,4,6,…,30).

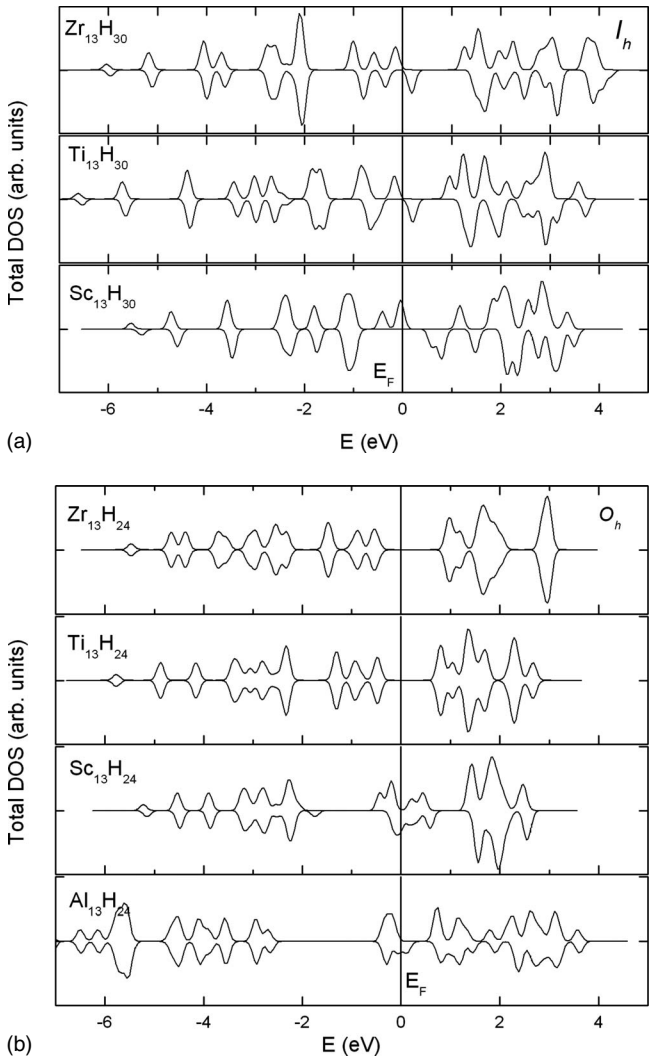

FIG. 4. Comparison of the total density of states of the hydrogenated I_h and O_h clusters.

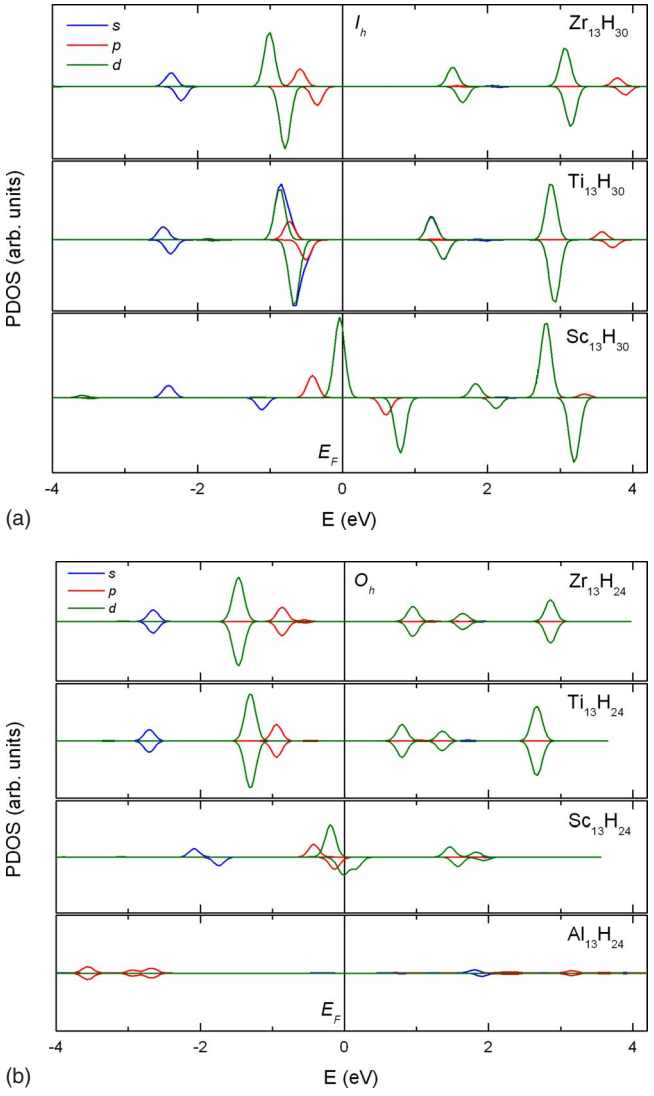

FIG. 5. (Color online) Comparison of the partial central-atom *s*-, *p*-, *d*-orbital density of states of the hydrogenated I_h and O_h clusters.

It has been shown earlier that the chemisorption energy of H_2 on transition metal surfaces can be correlated with the position of the *d*-band center relative to the Fermi level of the clean metal surface.[90–92] The chemisorption energy decreases as the *d*-band center is downshifted from the Fermi level. It will be useful to explore if this relationship is also satisfied for transition metal clusters at various degrees of hydrogen saturation. In Fig. 6(a) we present the chemisorption energy as a function of the *d*-band center for the $Ti_{13}H_n$ clusters, for $n=2-30$. All the hydrogens in the $Ti_{13}H_n$ ($n \leq 20$) clusters are of the μ_3 type and those of $Ti_{13}H_{30}$ are of μ_2 type.[47] The intervening $Ti_{13}H_{22}$, $Ti_{13}H_{24}$, $Ti_{13}H_{26}$, and $Ti_{13}H_{28}$ possess 16, 12, 10, and 5 μ_3 and 6, 12, 16, and 23 μ_2 hydrogens, respectively.[47] It can be seen that the linear relationship between chemisorption energy and the shift in *d*-band center is valid only for hydrogen concentrations of up to ten molecules. Beyond that, a shift in the position of the *d*-band center toward the Fermi level leads to a decrease in the magnitude of the chemisorption energy, opposite to that observed for clean metal surfaces. We believe that this is due to the significant decrease in chemisorption energy for $n>20$ at which a transition from μ_3 to μ_2 bonding occurs for the adsorbed hydrogen atoms. Figure 6(b) depicts the variation in the *d*-band center as a function of the adsorbed hydrogen atoms. It shows that the position of the *d*-band center varies by as much as 2.5 eV among the different $Ti_{13}H_n$ complexes. In Fig. 6(c) we show the chemisorption energy for the $M_{13}H_{20}$ and $M_{13}H_{30}$ clusters ($M=$Sc, Ti, Zr) as a function of the *d*-band center of the corresponding pure metal clusters. For the H_{20} clusters, the trend is similar to that exhibited by the $n<20$ clusters in Fig. 6(a), while the H_{30} clusters depict the behavior of the $n>20$ clusters in Fig. 6(a). The trends among the $M_{13}H_{20}$ and $M_{13}H_{30}$ clusters can also be understood by examining the partial *s*-, *p*-, *d*-orbital-resolved DOSs of the apex metal atoms shown in Fig. 7 for I_h and O_h clusters. The results illustrate that at high adsorbate concentrations or surface coverage, the correlation of the chemisorption energies with the *d*-band center of the pure metal cluster or nanoparticle may not be realistic but one has to take into account the changes in the *d*-orbital DOS

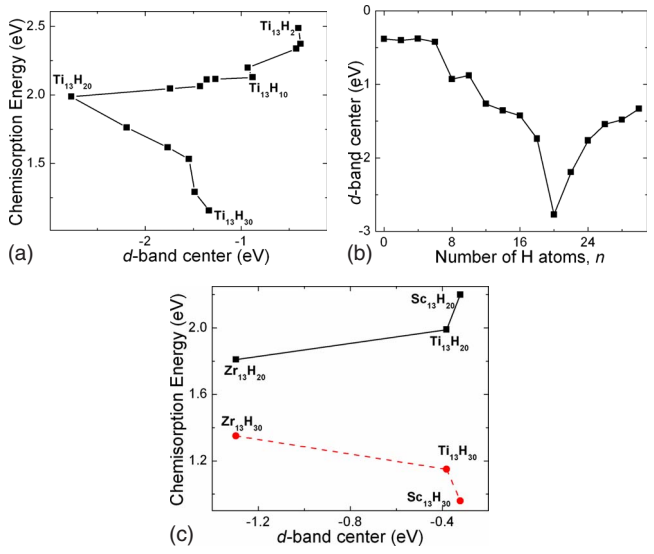

FIG. 6. (Color online) Plots of the (a) calculated d-band centers and the corresponding chemisorption (ΔE_{CE}) energies of each of the $Ti_{13}H_n$ ($n=2,4,6,\ldots,30$) clusters, (b) variations in the d-band center of $Ti_{13}H_n$ with an incremental addition of hydrogen atoms, and (c) calculated d-band centers of the pure M_{13} and the chemisorption (ΔE_{CE}) energies of the corresponding hydrogenated M_{13} clusters.

due to the presence of coadsorbed molecules. This may be especially important for small clusters and nanoparticles which can exhibit significant changes in the electronic properties due to the presence of chemisorbed molecules compared to extended metal surfaces.

D. Transition state of $M_{13}H_2$ clusters

Hitherto our discussion was focused on the properties of hydrogen saturated metal clusters. However in actual reactions, the nature of the transition state and the corresponding activation energies play a vital role in determining kinetics of hydrogen adsorption and saturation. A linear relationship between the activation energies and heats of reaction or dissociative chemisorption energy of H_2 has long been assumed to be valid. Such a behavior is referred to as Brønsted-Evans-Polanyi relationship in catalysis,[93,94] and it also holds for chemical reactions on clusters. Earlier studies have indicated that changes in the global structure of the parent metal cluster limits the validity of the Brønsted-Evans-Polanyi relationship for transition states.[95,96] However, for large clusters the global structures are largely unaffected by chemisorption.

Table V presents the activation energies, dissociative chemisorption energies, and the frequency of the M-H bond for the transition states of I_h $M_{13}H_2$ clusters. A total of 78 initial configurations were considered for the reactant geometries. Our earlier studies on small titanium clusters indicated that hydrogen dissociation takes place on top of a metal atom.[47,48] Hence in the construction of the reactant geometries, only the H-H and the metal-H_{CM} (H_{CM} is the center of mass of the hydrogen molecule) distances were varied. Thus

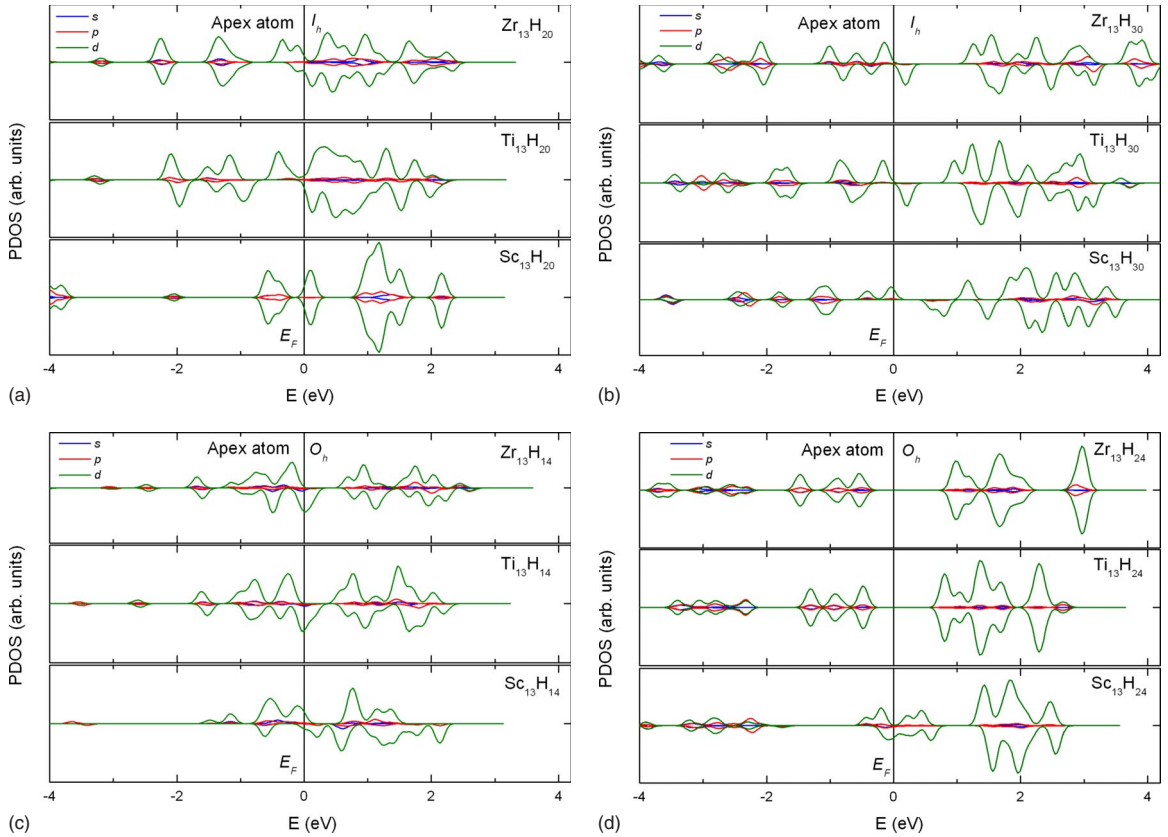

FIG. 7. (Color online) Comparison of the partial apex-atom s-, p-, d-orbital density of states of the hydrogenated I_h and O_h clusters.

TABLE V. The calculated activation energies, chemisorption energies, and imaginary frequencies of the transition states of I_h $M_{13}H_2$ clusters.

	Icosahedral clusters		
System	E_a (eV)	ΔE_{CE} (eV)	Imaginary frequency (cm^{-1})
$Sc_{13}H_2$	1.40	1.99	−1378.85
$Ti_{13}H_2$	2.34 (2.35[a])	2.49 (2.06[a])	−1417.89 (−1417.54 [a])
$Zr_{13}H_2$	1.56	2.26	−1423.61

[a]Results obtained using effective core potentials for titanium.

for generating the reactant geometries of the $Ti_{13}H_2$ clusters, the intermolecular Ti-H_{CM} distance was varied from 1.98 to 4.98 Å for a fixed H-H separation of 0.74 Å. The energy difference between the highest- and lowest-energy conformers of the resulting 13 reactant geometries was 0.6 eV. A plot of the chemisorption energy versus the activation energy shows that the results roughly conform to the Brønsted-Evans-Polanyi relation.[93,94,97,98] Table V shows that while the scandium cluster has the lowest activation energy, the titanium cluster has the highest chemisorption energy. A comparison of the reaction paths for the dissociative chemisorption of H_2 on the icosahedral M_{13} clusters is shown in Fig. 8(a). In this figure, we have also included results for dissociative chemisorption of H_2 on the icosahedral Al_{13} clusters.[21] While the dissociated hydrogen atoms preferentially occupy the most stable μ_3 sites in transition metal clusters, they are singly bonded to the aluminum atoms in the Al_{13} cluster. Both the activation energy and chemisorption energy for hydrogen adsorption are smaller for the aluminum cluster compared to the transition metal clusters. However for an ideal hydrogen storage material, low activation energies and moderate chemisorption energies are generally preferred. While none of the metal clusters investigated in this study are useful in this context, we have recently shown that suitable alloying could lead to materials with optimal chemisorption energies.[99]

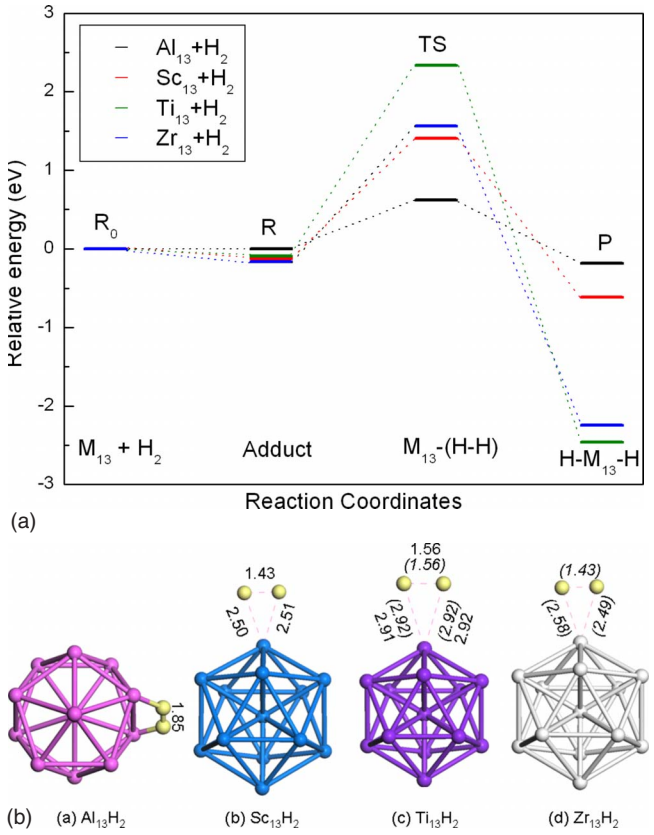

FIG. 8. (Color online) (a) The calculated reaction paths for dissociative chemisorption of a H_2 molecule on I_h M_{13} clusters of Al, Sc, Ti, and Zr, and, (b) the corresponding transition states. Transition state energy and geometry for $Al_{13}H_2$ in (a) and (b) are from Ref. 21. The geometric parameters enclosed in parentheses for $Ti_{13}H_2$ in (b) were obtained from calculations employing relativistic core potentials, while the rest were obtained from all-electron calculations.

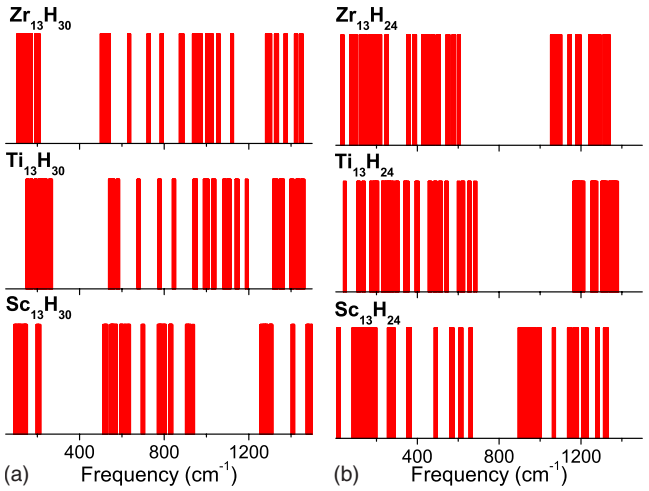

FIG. 9. (Color online) Stick plots of the calculated vibrational frequencies of the (a) icosahedral $Sc_{13}H_{30}$, $Ti_{13}H_{30}$, and $Zr_{13}H_{30}$, and (b) octahedral $Sc_{13}H_{24}$, $Ti_{13}H_{24}$, and $Zr_{13}H_{24}$ complexes.

Transition state geometries shown in [Fig. 8(b)] indicate that the titanium cluster enables the dissociation of hydrogen molecules at much longer distances than both zirconium and scandium. Viewed against the background of the activation and chemisorption energies, this indicates that titanium-containing materials could be more effective as catalysts in hydrogen storage. This suggests that clusters formed during ball milling of materials and complex metal hydrides containing titanium could have a hitherto unknown role in both modifying the activation energies of hydrogen dissociation and stabilizing the adsorbed hydrogen.

E. Vibrational frequencies

In a recent work, we have shown that hydrogens bound to multiple metal atoms are characterized by strong infrared (IR) active bands in the 1000–1500 cm^{-1} region.[99] The vibrational spectra of the hydrogen-saturated metal clusters investigated here, evaluated using VASP, are shown in Fig. 9.[100] The plots are depicted in stick format because the program does not enable the evaluation of IR intensities. Results show that irrespective of the nature of the metal species, distinct

bands are present in the 1200–1500 cm^{-1} region. It has been shown in our earlier work on titanium-containing clusters that these bands predominantly arise from hydrogens bound to multiple metal atoms.[48,99] Recent studies of hydrogen adsorption on 3*d* transition metal clusters also indicated the presence of strong IR peaks associated with hydrogens bound to multiple metal atoms.[101,102] In systems such as AlH_4^-, wherein the hydrogen atoms are singly bonded to the aluminum atom, one notes a total absence of peaks in the 1000–1500 cm^{-1} region.[103] Thus, the presence of frequencies in the 1000–1500 cm^{-1} region should provide an easy means to experimentally identify hydrogen-bonding motifs in hydrogenated metal clusters.

IV. SUMMARY AND CONCLUSIONS

We have performed first-principles DFT calculations of the geometric and electronic structures of Sc_{13}, Ti_{13}, and Zr_{13} clusters as well as the corresponding hydrogenated clusters at low and high hydrogen concentrations. Both icosahedral (I_h) and cuboctahedral (O_h) geometric structures were investigated. For comparison purpose, we have also carried out calculations on the corresponding Al_{13} clusters.

In contrast to Al_{13} clusters, the hydrogenated metal clusters were found to be energetically stable with the adsorbed hydrogen atom bonded to multiple metal atoms. At low hydrogen concentrations, the adsorbed hydrogen atoms occupy threefold sites in I_h symmetry and threefold and fourfold sites in O_h symmetry. At high H_2 concentrations, the dissociated hydrogen atoms occupy twofold sites in both I_h and O_h clusters. An increase in hydrogen concentration beyond 15 hydrogen molecules leads to the formation of hydrogenated M_{13} structures, wherein the hydrogen molecule is no longer dissociatively adsorbed. Our calculations show that the energetic stability of the parent metal cluster has little bearing on the chemisorption energies at high hydrogen saturation.

We have also examined the correlation between the position of the *d*-band center and the chemisorption energy as a function of the number of adsorbed hydrogen atoms. Our calculations show that at low hydrogen concentrations the chemisorption energy decreases linearly with the shift in the location of the *d*-band relative to the Fermi level of the pure cluster or the hydrogenated clusters, in agreement with previous studies of chemisorption of a single H_2 molecule on clean transition metal surfaces. This trend persists up to 20 hydrogen atoms for the $M_{13}H_n$ clusters but it reverses for $n > 20$. The reversal of the slope of the plot of *d*-band center versus chemisorption energy for $n > 20$ could be attributed to a transition from μ_3 to μ_2 bonding for the $M_{13}H_n$ clusters. This might also apply to high concentrations of other adsorbates in nanocatalysis.

To gain insights into the chemisorption process, the transition state structures, activation energies, and reaction paths for H_2 dissociation on the icosahedral M_{13} clusters have been determined. While the activation energies for hydrogen adsorption on the scandium and zirconium clusters are comparable, the highest chemisorption energy is exhibited by the titanium clusters. This trend is however reversed at high hydrogen concentrations, wherein the zirconium clusters exhibit the highest chemisorption energies. The energies of the transition states of these systems are found to be consistent with the empirical Brønsted-Evans-Polanyi relationship.

An analysis of the density of states of unfilled *d* orbitals of the metal atoms shows that the central metal atom plays a vital role in stabilizing the adsorbed hydrogen atoms. Though the metal clusters investigated in this study may not be suitable for hydrogen storage due to their high chemisorption energies, it is likely that suitable alloying could lead to clusters with optimal chemisorption energies.

The calculated vibrational spectra of the hydrogen-saturated metal clusters indicate that they exhibit characteristic bands associated with hydrogen multicenter bonds in the 1000–1500 cm^{-1} region. The presence of strong IR bands in this frequency regime may be used to experimentally identify bonding patterns in hydrogen-saturated metal clusters.

ACKNOWLEDGMENT

This work was financially supported by Department of Energy (Grant No. DE-FG36-05G085028).

*tarakesh@unlv.nevada.edu
†naduvala@unlv.nevada.edu

[1] M. Turner, V. B. Golovko, O. P. H. Vaughan, P. Abdulkin, A. Berenguer-Murcia, M. S. Tikhov, B. F. G. Johnson, and R. M. Lambert, Nature (London) **454**, 981 (2008).
[2] A. A. Herzing, C. J. Kiely, A. F. Carley, P. Landon, and G. J. Hutchings, Science **321**, 1331 (2008).
[3] S. C. Warren, L. S. Messina, L. S. Slaughter, M. Kamperman, Q. Zhou, S. M. Gruner, F. J. DiSalvo, and U. Wiesner, Science **320**, 1748 (2008).
[4] A. W. Castleman and P. Jena, Proc. Natl. Acad. Sci. U.S.A. **103**, 10554 (2006).
[5] A. Züttel, Naturwiss. **91**, 157 (2004).
[6] Y. Isobe, M. Yamauchi, R. Ikeda, and H. Kitagawa, Synth. Met. **135-136**, 757 (2003).
[7] W.-Q. Deng, X. Xu, and W. A. Goddard, Phys. Rev. Lett. **92**, 166103 (2004).
[8] T. Yildirim and S. Ciraci, Phys. Rev. Lett. **94**, 175501 (2005).
[9] Q. Sun, P. Jena, Q. Wang, and M. Marquez, J. Am. Chem. Soc. **128**, 9741 (2006).
[10] B. Kiran, A. K. Kandalam, and P. Jena, J. Chem. Phys. **124**, 224703 (2006).
[11] P. F. Weck, T. J. Dhilip Kumar, E. Kim, and N. Balakrishnan, J. Chem. Phys. **126**, 094703 (2007).
[12] Y. Zhao, Y.-H. Kim, A. C. Dillon, M. J. Heben, and S. B. Zhang, Phys. Rev. Lett. **94**, 155504 (2005).
[13] Q. Sun, Q. Wang, P. Jena, and Y. Kawazoe, J. Am. Chem. Soc. **127**, 14582 (2005).

[14] C. Zhou, S. Yao, J. Wu, R. C. Forrey, L. Chen, A. Tachibana, and H. Cheng, Phys. Chem. Chem. Phys. **10**, 5445 (2008).
[15] C. Zhou, J. Wu, A. Nie, R. C. Forrey, A. Tachibana, and H. Cheng, J. Phys. Chem. C **111**, 12773 (2007).
[16] S. Satyapal, J. Petrovic, C. Read, G. Thomas, and G. Ordaz, Catal. Today **120**, 246 (2007); U.S. Department of Energy, Hydrogen, Fuel Cells & Infrastructure Technologies Program: Multi-Year Research, Development and Demonstration Plan, April 2007, Chap. 3, http://www1.eere.energy.gov/hydrogenandfuelcells/mypp/
[17] A. Pundt and R. Kirchheim, Annu. Rev. Mater. Res. **36**, 555 (2006).
[18] E. Bus and J. A. van Bokhoven, Phys. Chem. Chem. Phys. **9**, 2894 (2007).
[19] A. Züttel, C. Nützenagel, G. Schmid, C. Emmenegger, P. Sudan, and L. Schlapbach, Appl. Surf. Sci. **162-163**, 571 (2000).
[20] M. N. Huda and L. Kleinman, Phys. Rev. B **74**, 195407 (2006).
[21] I. Yarovsky and A. Goldberg, Mol. Simul. **31**, 475 (2005).
[22] A. Goldberg and I. Yarovsky, Phys. Rev. B **75**, 195403 (2007).
[23] B. Kiran, P. Jena, X. Li, A. Grubisic, S. T. Stokes, G. F. Ganteför, K. H. Bowen, R. Burgert, and H. Schnockel, Phys. Rev. Lett. **98**, 256802 (2007).
[24] B. Bogdanović and M. Schwickardi, J. Alloys Compd. **253-254**, 1 (1997).
[25] B. Bogdanović, M. Felderhoff, S. Kaskel, A. Pommerin, K. Schlichte, and F. Schüth, Adv. Mater. (Weinheim, Ger.) **15**, 1012 (2003).
[26] B. Bogdanović, M. Felderhoff, A. Pommerin, F. Schüth, and N. Spielkamp, Adv. Mater. (Weinheim, Ger.) **18**, 1198 (2006).
[27] R. A. Zidan, S. Takara, A. G. Hee, and C. M. Jensen, J. Alloys Compd. **285**, 119 (1999).
[28] T. Wang, J. Wang, A. D. Ebner, and J. A. Ritter, J. Alloys Compd. **450**, 293 (2008).
[29] C. Weidenthaler, A. Pommmerin, M. Felderhoff, B. Bogadanovic, and F. Schüth, Phys. Chem. Chem. Phys. **5**, 5149 (2003).
[30] M. Fichtner, O. Fuhr, O. Kircher, and J. Rothe, Nanotechnology **14**, 778 (2003).
[31] C. P. Baldé, B. P. C. Hereijgers, J. H. Bitter, and K. P. de Jong, J. Am. Chem. Soc. **130**, 6761 (2008).
[32] C. P. Baldé, B. P. C. Hereijgers, J. H. Bitter, and K. P. de Jong, Angew. Chem., Int. Ed. **45**, 3501 (2006).
[33] A. Blomqvist, C. Moysès Araùjo, P. Jena, and R. Ahuja, Appl. Phys. Lett. **90**, 141904 (2007).
[34] S. Chaudhuri and J. T. Muckerman, J. Phys. Chem. B **109**, 6952 (2005).
[35] S. Chaudhuri, J. Graetz, A. Ignatov, J. J. Reilly, and J. T. Muckerman, J. Am. Chem. Soc. **128**, 11404 (2006).
[36] C. M. Araújo, R. Ahuja, J. M. O. Guillén, and P. Jena, Appl. Phys. Lett. **86**, 251913 (2005).
[37] C. M. Araújo, S. Li, R. Ahuja, and P. Jena, Phys. Rev. B **72**, 165101 (2005).
[38] S. Li, P. Jena, and R. Ahuja, Phys. Rev. B **73**, 214107 (2006).
[39] A. Marashdeh, R. A. Olsen, O. M. Løvvik, and G.-J. Kroes, Chem. Phys. Lett. **426**, 180 (2006).
[40] O. M. Lovvik and S. Opalka, Phys. Rev. B **71**, 054103 (2005).
[41] J. Íñiguez and T. Yildrim, Appl. Phys. Lett. **86**, 103109 (2005).
[42] P. Wang, X.-D. Kang, and H.-M. Cheng, J. Phys. Chem. B **109**, 20131 (2005).
[43] J. Liu and Q. Ge, J. Phys. Chem. B **110**, 25863 (2006).
[44] J. Liu and Q. Ge, Chem. Commun. (Cambridge) **2006**, 1822.
[45] J. Liu and Q. Ge, J. Alloys Compd. **446-447**, 267 (2007).
[46] T. J. Dhilip Kumar, P. F. Weck, and N. Balakrishnan, J. Phys. Chem. C **111**, 7494 (2007).
[47] T. J. Dhilip Kumar, P. Tarakeshwar, and N. Balakrishnan, J. Chem. Phys. **128**, 194714 (2008).
[48] P. Tarakeshwar, T. J. Dhilip Kumar, and N. Balakrishnan, J. Phys. Chem. A **112**, 2846 (2008).
[49] S. Burkart, N. Blessing, and G. Ganteför, Phys. Rev. B **60**, 15639 (1999).
[50] Y. D. Kim and G. Ganteför, J. Mol. Struct. **692**, 139 (2004).
[51] M. Salazar-Villanueva, P. H. Hernández-Tejeda, U. Pal, J. F. Rivas-Silva, J. I. Rodríguez-Mora, and J. A. Ascencio, J. Phys. Chem. A **110**, 10274 (2006).
[52] J. Wang, Phys. Rev. B **75**, 155422 (2007).
[53] H. K. Yuan, H. Chen, A. S. Ahmed, and J. F. Zhang, Phys. Rev. B **74**, 144434 (2006).
[54] C.-C. Wang, R.-N. Zhoa, and J.-G. Han, J. Chem. Phys. **124**, 194301 (2006).
[55] L. Lian, C.-X. Su, and P. B. Armentrout, J. Chem. Phys. **97**, 4084 (1992).
[56] M. Castro, S.-R. Liu, H.-J. Zhai, and L.-S. Wang, J. Chem. Phys. **118**, 2116 (2003).
[57] F. Baletto and R. Ferrando, Rev. Mod. Phys. **77**, 371 (2005).
[58] Y. Sun, M. Zhang, and R. Fournier, Phys. Rev. B **77**, 075435 (2008).
[59] S. Alexander and J. McTague, Phys. Rev. Lett. **41**, 702 (1978).
[60] J. P. Perdew, J. A. Chevary, S. H. Vosko, K. A. Jackson, M. R. Pederson, D. J. Singh, and C. Fiolhais, Phys. Rev. B **46**, 6671 (1992).
[61] G. Kresse and J. Hafner, Phys. Rev. B **47**, 558 (1993).
[62] G. Kresse and J. Hafner, Phys. Rev. B **49**, 14251 (1994).
[63] G. Kresse and J. Furthmüller, Comput. Mater. Sci. **6**, 15 (1996).
[64] G. Kresse and J. Furthmüller, Phys. Rev. B **54**, 11169 (1996).
[65] P. E. Blochl, Phys. Rev. B **50**, 17953 (1994).
[66] G. Kresse and D. Joubert, Phys. Rev. B **59**, 1758 (1999).
[67] L. G. Hector, Jr. and J. F. Herbst, J. Phys.: Condens. Matter **20**, 064229 (2008).
[68] T. A. Halgren and W. N. Lipscomb, Chem. Phys. Lett. **49**, 225 (1977).
[69] B. Delley, J. Chem. Phys. **92**, 508 (1990); **113**, 7756 (2000).
[70] S.-Y. Wang, W. Duan, D.-L. Zhao, and C.-Y. Wang, Phys. Rev. B **65**, 165424 (2002).
[71] B. Lee and G. W. Lee, J. Chem. Phys. **129**, 024711 (2008).
[72] J. R. Lombardi and B. Davis, Chem. Rev. (Washington, D.C.) **102**, 2431 (2002).
[73] P. Bobadova-Parvanova, K. A. Jackson, S. Srinivas, and M. Horoi, Phys. Rev. B **66**, 195402 (2002).
[74] B. V. Reddy, S. N. Khanna, and B. I. Dunlap, Phys. Rev. Lett. **70**, 3323 (1993).
[75] N. Watari and S. Ohnishi, J. Chem. Phys. **106**, 7531 (1997).
[76] M. Okumura, Y. Kitagawa, M. Haruta, and K. Yamaguchi, Appl. Catal., A **291**, 37 (2005).
[77] H.-P. Cheng, R. S. Berry, and R. L. Whetten, Phys. Rev. B **43**, 10647 (1991).
[78] D. J. Henry, A. Varano, and I. Yarovsky, J. Phys. Chem. A **112**, 9835 (2008).
[79] X. G. Gong and V. Kumar, Phys. Rev. Lett. **70**, 2078 (1993).
[80] A. Mañanes, F. Duque, F. Méndez, M. J. López, and J. A. Alonso, J. Chem. Phys. **119**, 5128 (2003).
[81] L. Wang and D. D. Johnson, J. Am. Chem. Soc. **129**, 3658

(2007).
[82] M. K. Oudenhuijzen, J. A. van Bokhoven, J. T. Miller, D. E. Ramaker, and D. C. Koningsberger, J. Am. Chem. Soc. **127**, 1530 (2005).
[83] K. Hofmann, M. H. Prosenc, and B. R. Albert, Chem. Commun. (Cambridge) **2007**, 3097.
[84] M. Yousufuddin, M. Gutmann, J. Baldamus, O. Tardif, Z. Hou, S. A. Mason, G. J. McIntyre, and R. Bau, J. Am. Chem. Soc. **130**, 3888 (2008).
[85] M. L. McKee, M. Bühl, O. Charkin, and P. v. R. Schleyer, Inorg. Chem. **32**, 4549 (1993).
[86] K. Balasubramanian and C. Ravimohan, J. Chem. Phys. **92**, 3659 (1990).
[87] D. Dai and K. Balasubramanian, Chem. Phys. Lett. **231**, 352 (1994); **193**, 565 (1992).
[88] D. Majumdar and K. Balasubramanian, Chem. Phys. Lett. **279**, 403 (1997).
[89] D. Hobbs, G. Kresse, and J. Hafner, Phys. Rev. B **62**, 11556 (2000).
[90] B. Hammer and J. K. Nørskov, Adv. Catal. **45**, 71 (2000).
[91] V. Pallassana, M. Neurock, L. B. Hansen, B. Hammer, and J. K. Norskov, Phys. Rev. B **60**, 6146 (1999).
[92] F. Abild-Pedersen, J. Greeley, and J. K. Nørskov, Catal. Lett. **105**, 9 (2005).
[93] J. N. Brönsted, Chem. Rev. (Washington, D.C.) **5**, 231 (1928).
[94] M. G. Evans and N. P. Polanyi, Trans. Faraday Soc. **34**, 11 (1938).
[95] G. H. Guvelioglu, P. Ma, X. He, R. C. Forrey, and H. Cheng, Phys. Rev. Lett. **94**, 026103 (2005).
[96] R. C. Forrey, G. H. Guvelioglu, P. Ma, X. He, and H. Cheng, Phys. Rev. B **73**, 155437 (2006).
[97] J. K. Nørskov, T. Bligaard, A. Logadottir, S. Bahn, L. B. Hansen, M. Bollinger, H. Bengaard, B. Hammer, Z. Sljivancanin, M. Mavrikakis, Y. Xu, S. Dahl, and C. J. Jacobsen, J. Catal. **209**, 275 (2002).
[98] A. Michaelides, Z. P. Liu, C. J. Zhang, A. Alavi, D. A. King, and P. Hu, J. Am. Chem. Soc. **125**, 3704 (2003).
[99] P. Tarakeshwar, T. J. Dhilip Kumar, and N. Balakrishnan, J. Chem. Phys. **130**, 114301 (2009).
[100] Frequency evaluations using VASP are prone to both DFT-related and numerical errors. These errors can be mitigated to a large extent by using extremely small time steps and high precision at the cost of very large computational effort. At high precision and a small time step, all the hydrogen-saturated titanium and zirconium clusters exhibit no imaginary frequencies. However, the corresponding scandium clusters exhibit extremely small imaginary frequencies. We believe an even smaller time step would yield all positive frequencies for the scandium systems but the computational effort would be prohibitively expensive.
[101] I. Swart, A. Fielicke, B. Redlich, G. Meijer, B. M. Weckhuysen, and F. M. F. de Groot, J. Am. Chem. Soc. **129**, 2516 (2007).
[102] I. Swart, F. M. F. de Groot, B. M. Weckhuysen, P. Gruene, G. Meijer, and A. Fielicke, J. Phys. Chem. A **112**, 1139 (2008).
[103] P. Pullumbi, Y. Bouteiller, and Y. Manceron, J. Chem. Phys. **101**, 3610 (1994).